International Journal of Science and Engineering Applications
Volume 15-Issue 09, 103 – 106, 2026, ISSN:- 2319 - 7560
DOI: 10.7753/IJSEA1509.1020

Simulation of Field-Oriented Control with Dual Fuzzy Self-Tuning PID for a Two-Phase Hybrid Stepping Motor

Jun-hao Chen
School of Electronic Information and Electrical Engineering
Yangtze University
Jingzhou, China

Shi-ping Sun
School of Electronic Information and Electrical Engineering
Yangtze University
Jingzhou, China

Abstract: To solve the problems of low-frequency oscillation, high-frequency step-out and torque decline in the open-loop drive of a two-phase hybrid stepping motor, this paper establishes its mathematical model and designs three progressively optimized control schemes, namely open-loop microstepping control, field-oriented control (FOC) with conventional three-loop PID, and FOC with dual fuzzy self-tuning PID. The motor model and the coordinate transformation are derived, and the three schemes are implemented in Matlab/Simulink. Position-step and 0.5 s load-disturbance tests are carried out for comparison. Simulation results show that FOC decouples the flux and torque components and markedly sinusoidalizes the phase current; after the fuzzy self-tuning PID is introduced into the position and speed loops, the position drop under load disturbance is reduced from 0.20 rad to 0.12 rad, the recovery time is shortened from 0.35 s to 0.20 s, and the overshoot is reduced from 3.2% to 3.0%, demonstrating the adaptability of fuzzy control to parameter variation and external disturbance.

Keywords: hybrid stepping motor; field-oriented control; fuzzy self-tuning PID; microstepping; three-loop control; Simulink

1. INTRODUCTION

Stepping motors are widely used in CNC machines, textile machinery, 3D printers and robot joints because they can be driven directly by digital signals, have no cumulative positioning error, and are simple and inexpensive. However, conventional open-loop stepping drives feed square- or staircase-wave currents to the windings, which causes large current harmonics, free oscillation of the rotor around the equilibrium point at low speed, and poor load capability or even step-out at high speed [1]-[3]. Microstepping reduces the torque ripple by making the phase current approximately sinusoidal, but it still regulates the current in the stationary frame and does not fundamentally remove the step-out problems [4]-[5].

Field-oriented control (FOC) borrows the idea of permanent-magnet synchronous motor control: through coordinate transformation the currents are decoupled into the rotating d-q frame so that the torque- and flux-producing components are controlled independently, which significantly improves the current waveform and the high-speed performance. Reference [6] proposed a two-phase SVPWM based vector control system for a two-phase hybrid stepping motor and verified the improvement on oscillation and step-out, but its PI gains are fixed and cannot adapt to load disturbance and parameter variation. The fuzzy PID controller takes the error and its rate of change as inputs and tunes Kp, Ki and Kd online through fuzzy inference without relying on an accurate model, which is an effective way to improve robustness [7].

In this paper, taking a two-phase hybrid stepping motor as the plant, the control scheme is optimized progressively along the route of open-loop microstepping control, FOC with three-loop PID, and FOC with dual fuzzy PID. The mathematical model and the coordinate transformation are derived, and the three schemes are built in Simulink and compared through a position step with a load disturbance suddenly applied at 0.5 s.

2. MATHEMATICAL MODEL OF THE MOTOR

2.1 Inductance and Flux Equations

A two-phase hybrid stepping motor can be regarded as a two-phase permanent-magnet synchronous motor whose A and B windings are spatially orthogonal, with the number of pole pairs p = 50 (corresponding to a 1.8° step angle). Neglecting the leakage flux and the higher-order reluctance terms, the phase self-inductances and the mutual inductance are

$$L_{AA} = L_0 - L_2\cdot\cos(2\theta_e),\quad L_{BB} = L_0 + L_2\cdot\cos(2\theta_e),\quad M_{AB} = -L_2\cdot\sin(2\theta_e) \tag{1}$$

where L_{AA} and L_{BB} are the self-inductances of the A and B phases, M_{AB} is the mutual inductance between the two phases, L_0 and L_2 are the constant and fundamental components of the winding inductance, and θ_e is the electrical angle.

2.2 Voltage Equations

From the flux equations, the voltage equations of the two windings in the stationary α-β frame are

$$v_\alpha = R\cdot i_\alpha + L\cdot(di_\alpha/dt) - \lambda_m\cdot\omega_e\cdot\sin\theta_e \tag{2}$$

$$v_\beta = R\cdot i_\beta + L\cdot(di_\beta/dt) + \lambda_m\cdot\omega_e\cdot\cos\theta_e \tag{3}$$

where R is the phase resistance, L is the phase inductance, λ_m is the amplitude of the permanent-magnet flux linkage, ω_e is the electrical angular velocity, and i_α, i_β, v_α, v_β are the currents and voltages in the stationary frame. The terms $-\lambda_m\omega_e\cdot\sin\theta_e$ and $\lambda_m\omega_e\cdot\cos\theta_e$ are the back-EMF terms.

2.3 Torque and Mechanical Motion Equations

The electromagnetic torque is produced by the interaction between the phase currents and the permanent-magnet flux:

$$T_e = p\cdot\lambda_m\cdot(i_\beta\cdot\cos\theta_e - i_\alpha\cdot\sin\theta_e) \tag{4}$$

The mechanical motion is described by

$$J\cdot(d\omega_m/dt) = T_e - T_L - B\cdot\omega_m,\quad d\theta_m/dt = \omega_m,\quad \theta_e = p\cdot\theta_m \tag{5}$$

where T_e and T_L are the electromagnetic and load torques, J is the rotor inertia, B is the viscous damping coefficient, and ω_m and θ_m are the mechanical angular velocity and position. The motor parameters used in this paper are listed in Table 1.

Table 1. Main parameters of the motor

Parameter	Value	Parameter	Value
Pole pairs p	50	Phase resistance R	1.5 Ω
Phase inductance L	12 mH	Flux linkage λm	0.00534 Wb

Rotor inertia J	1×10^{-4} kg·m²	Damping B	1×10^{-4} N·m·s/rad
DC bus voltage Vdc	24 V	Max q-axis current Imax	2 A

3. FIELD-ORIENTED CONTROL AND CONTROL SCHEMES

3.1 Coordinate Transformation and FOC Principle

To convert the AC quantities in the stationary frame into DC quantities in the rotating frame, the Park transform and its inverse are introduced:

$$[i_d, i_q]^T = [\cos\theta_e \ \ \sin\theta_e; -\sin\theta_e \ \ \cos\theta_e]\cdot[i_\alpha, i_\beta]^T \quad (6)$$

$$[v_\alpha, v_\beta]^T = [\cos\theta_e \ \ -\sin\theta_e; \sin\theta_e \ \ \cos\theta_e]\cdot[v_d, v_q]^T \quad (7)$$

Under the id = 0 control strategy, the electromagnetic torque reduces to

$$T_e = p\cdot\lambda_m\cdot i_q \quad (8)$$

so that the torque is linearly related to the q-axis current and a DC-motor-like decoupled control is achieved.

3.2 Scheme I: Open-Loop Microstepping Control

Scheme I generates the two-phase sinusoidal current references directly in the stationary frame, $i_A^* = I_{amp}\cdot\sin(\omega_e\cdot t)$ and $i_B^* = I_{amp}\cdot\cos(\omega_e\cdot t)$, and uses current-loop PI controllers to make the actual currents track the references. Since the reference frequency is fixed by the electrical angle and no rotor position feedback is used, it is an open-loop control. The current loop is designed by the bandwidth method with the target bandwidth $\omega_c = 2\pi\cdot500$ rad/s:

$$K_p = L\cdot\omega_c, \quad K_i = R\cdot\omega_c \quad (9)$$

Substituting L = 12 mH and R = 1.5 Ω gives Kp ≈ 37.7 and Ki ≈ 4712. The structure of Scheme I is shown in Fig. 1.

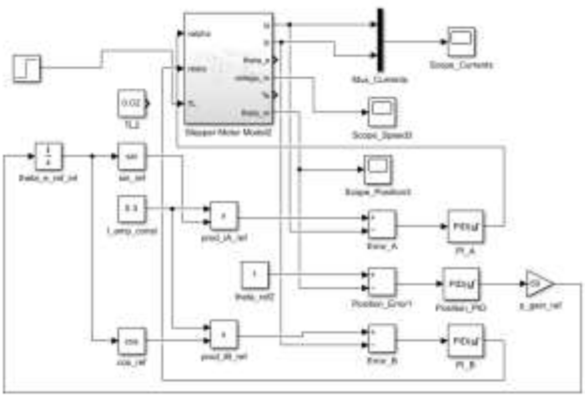

Figure 1. Scheme I: open-loop microstepping control

3.3 Scheme II: FOC with Three-Loop PID Control

Scheme II introduces FOC and a cascaded three-loop structure: the position-loop PI outputs the speed reference ω*, the speed-loop PI outputs the q-axis current reference iq*, and the d-axis current reference is set to id* = 0. The d-q current errors are regulated by PI controllers and then transformed by the inverse Park transform into vα and vβ. To guarantee stability, the bandwidths of the three loops decrease successively (current loop 500 Hz, speed loop 50 Hz, position loop 5 Hz). The position PI gains are Kp = 15 and Ki = 1, the speed PI gains are Kp = 0.05 and Ki = 2, and the current PI gains are the same as in Scheme I. The structure is shown in Fig. 2.

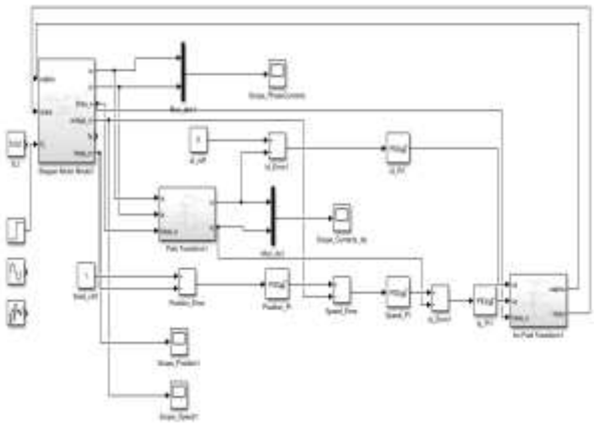

Figure 2. Scheme II: FOC with three-loop PID control

3.4 Scheme III: FOC with Dual Fuzzy Self-Tuning PID Control

3.4.1 Structure of the fuzzy self-tuning PID

Scheme III keeps the FOC structure of Scheme II but replaces the fixed-gain PID in the position and speed loops with fuzzy self-tuning PID, while the current loop remains a conventional PI. The fuzzy PID takes the error e and its rate of change ec as inputs and outputs the corrections ΔKp, ΔKi and ΔKd to adjust the PID gains online:

$$K_p = K_{p0} + \Delta K_p, \quad K_i = K_{i0} + \Delta K_i, \quad K_d = K_{d0} + \Delta K_d \quad (10)$$

so that the control intensity adapts to different error states. The structure is shown in Fig. 3, where the inner structure of the fuzzy self-tuning PID is also illustrated.

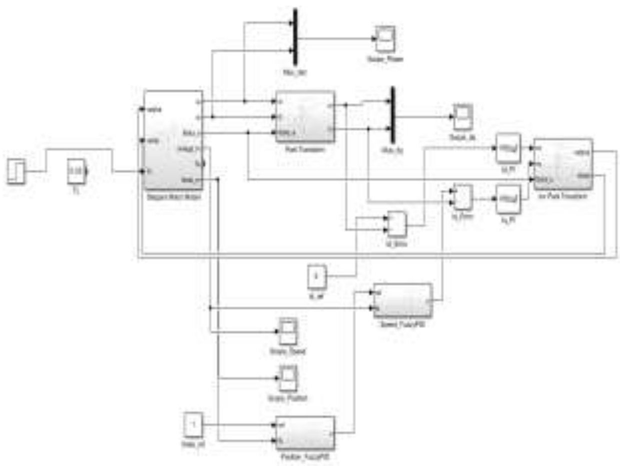

Figure 3. Scheme III: FOC with dual fuzzy self-tuning PID control

3.4.2 Fuzzification and membership functions

Both fuzzy controllers use Mamdani inference. The universes of the inputs e, ec and the outputs ΔKp, ΔKi, ΔKd are all normalized to [−3, 3], and each variable is partitioned into seven fuzzy sets {NB, NM, NS, ZO, PS, PM, PB} with triangular membership functions:

$$\mu(x) = \max(0, \min((x-a)/(b-a), (c-x)/(c-b))) \quad (11)$$

where a, b and c are the left, peak and right points of the triangle. The actual error and its rate of change are mapped into the normalized universe through the scaling factors

$$Ke = 3/|e\_max|, \quad Kec = 3/|ec\_max| \qquad (12)$$

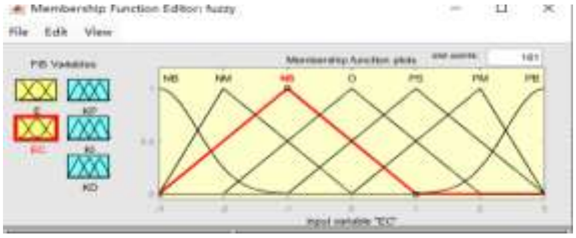

Figure 4. Membership function

3.4.3 Fuzzy rule base

The rule base consists of 49 IF-THEN rules covering all 7×7 combinations of e and ec. The rules follow the principle that when the error is large a large Kp is used to speed up the response, when the error is small a large Ki is used to eliminate the steady-state error, and Kd is adjusted according to the rate of error change to suppress overshoot. Table 2 lists the rules in the form of ΔKp/ΔKi/ΔKd.

Table 2. Fuzzy rule base (ΔKp/ΔKi/ΔKd)

e \ ec	NB	NM	NS	ZO	PS	PM	PB
NB	PB/NB/PS	PB/NB/NS	PM/NM/NB	PM/NM/NB	PS/NS/NB	ZO/ZO/NM	ZO/ZO/PS
NM	PB/NB/PS	PB/NB/NS	PM/NM/NS	PS/NS/NS	PS/NS/ZO	ZO/ZO/NS	ZO/ZO/PM
NS	PB/NM/NB	PM/NM/NB	PM/NS/NM	PS/NS/NS	ZO/ZO/ZO	NS/PS/PS	NM/PS/PM
ZO	PB/NM/NB	PS/NS/NM	PM/NS/NM	ZO/ZO/NS	NS/PS/ZO	NM/PS/PS	NM/PM/PM
PS	PM/NS/NB	PS/NS/NM	ZO/ZO/NS	NS/PS/NS	NS/PS/ZO	NM/PS/PS	NM/PM/PS
PM	PS/ZO/NM	ZO/ZO/NS	NS/PS/NS	NM/PM/NS	NM/PM/ZO	NM/PB/PS	NB/PB/PS
PB	ZO/ZO/PS	NS/ZO/ZO	NS/PS/ZO	NM/PM/ZO	NM/PB/ZO	NB/PB/PB	NB/PB/PB

3.4.4 Defuzzification and output scaling

The Mamdani inference uses the min operator for implication and the max operator for aggregation. The crisp output is obtained by the centroid defuzzification

$$y0 = \Sigma\, \mu i \cdot yi \,/\, \Sigma\, \mu i \qquad (13)$$

where μi is the degree of activation of the i-th rule and yi is the centroid of the corresponding output fuzzy set. The output scaling factors map the normalized ΔKp, ΔKi and ΔKd to their actual ranges. For the position loop, Ke = 3, Kec = 0.1, Kp0 = 15, Kd0 = 0.3, and the scaling factors of ΔKp/ΔKi/ΔKd are [1.5, 0.1, 0.03]; for the speed loop, Ke = 0.1, Kec = 0.003, Kp0 = 0.05, Ki0 = 2, Kd0 = 0.001, and the scaling factors are [0.005, 0.2, 0.0001]. The fuzzy controllers are implemented in discrete form with a sampling period of 1×10^{-4} s.

4. SIMULATION RESULTS AND ANALYSIS

4.1 Simulation Setup

The three schemes are built in Simulink with the fixed-step ode4 solver and a step size of 1×10^{-6} s. The position reference is a 1 rad step, and a load torque of 0.05 N·m is suddenly applied at 0.5 s. The simulation time is 1.5 s for Scheme I and 1.0 s for Schemes II and III.

4.2 Current and Speed Responses

Fig. 5 compares the phase currents of Schemes I and II. In Scheme I the phase current oscillates noticeably at the beginning and then becomes stable, indicating that the open-loop control is sensitive to the initial state and has high harmonic content; in Scheme II the phase current becomes smooth and sinusoidal without initial oscillation, which verifies the improvement of the current quality brought by coordinate transformation. For the speed response, Scheme I shows a start-stop process with oscillation, while the speed responses of Schemes II and III are much smoother.

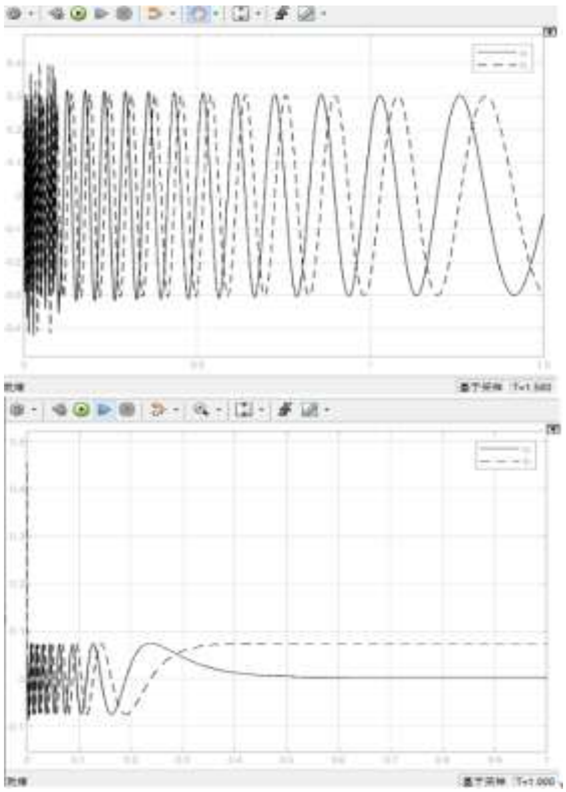

Figure 5. Phase current waveforms (top: Scheme I; bottom: Scheme II)

4.3 Position Response and Anti-Disturbance Performance

Figure 6 shows the position (top) and speed (bottom) responses for Scheme 1. Although the position in Scheme 1 can reach the target, there's a risk of misstep due to no position feedback. Figures 7 and 8 compare the speed and position responses for Schemes 2 and 3. The position of Scheme II rises smoothly to 1 rad with an overshoot of about 3.2% and a settling time of about 0.32 s; when the load is suddenly applied at 0.5 s, the position drops by about 0.20 rad and recovers in about 0.35 s. The position of Scheme III has an overshoot of about 3.0% and a settling time of about 0.30 s; under the same disturbance the position drop is about 0.12 rad and the recovery time is about 0.20 s.

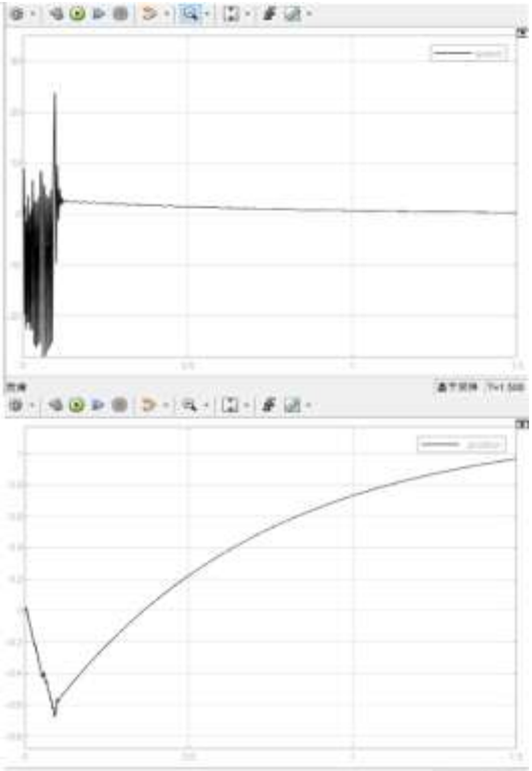

Figure 6. Position and speed responses of Scheme I

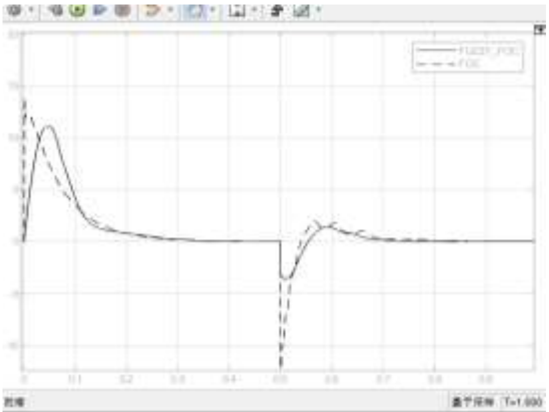

Figure 7. Comparison of the speed responses of Scheme II and Scheme III

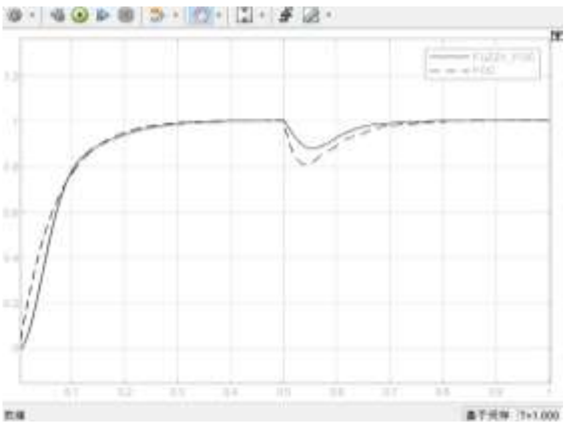

Figure 8. Comparison of the position responses of Scheme II and Scheme III

The overshoot and the settling time are defined as

$$\sigma = (M_p - y_\infty)/y_\infty \times 100\%, \quad |y(t_s) - y_\infty| \le 2\% \cdot y_\infty \quad (14)$$

where Mp is the peak value and y_∞ is the steady-state value. The performance indices of the three schemes are compared in Table 3.

Table 3. Performance comparison of the three schemes

Index	Scheme I	Scheme II	Scheme III
Current waveform	Initial oscillation	Smooth sinusoidal	Smooth sinusoidal
Overshoot	—	3.2%	3.0%
Settling time	—	0.32 s	0.30 s
Load drop	Step-out	0.20 rad	0.12 rad
Recovery time	—	0.35 s	0.20 s
Parameter adaption	No	No	Yes

It can be seen from Table 3 that the performance improves progressively from Scheme I to Scheme III. After FOC is introduced, the current becomes sinusoidal and the position accuracy and anti-disturbance ability are improved; after the fuzzy PID is introduced, the position drop under load disturbance is reduced by 40% and the recovery time is shortened by 43%, which significantly improves the robustness while maintaining the steady-state accuracy.

5. CONCLUSION

This paper establishes the mathematical model of a two-phase hybrid stepping motor and designs three control schemes along the route of open-loop microstepping control, FOC with three-loop PID, and FOC with dual fuzzy PID, which are compared by Simulink simulation. The results show that FOC decouples the flux and torque components through the Park transform and makes the phase current significantly sinusoidal; the three-loop cascade structure achieves precise closed-loop control of position, speed and current; and the fuzzy self-tuning PID reduces the position drop and the recovery time under load disturbance by 40% and 43% respectively compared with the conventional PID, significantly improving the robustness. Future work includes adaptive neuro-fuzzy inference systems, sensorless FOC and algorithm implementation on DSP/FPGA platforms.

6. REFERENCES

[1] Z. Liu, G. Chang and G. Xu, "Vector control system of two-phase hybrid stepping motor," Light Industry Machinery, vol. 38, no. 5, pp. 55-62, 2020.

[2] K. M. Le, H. Van Hoang and J. W. Jeon, "An advanced closed-loop control to improve the performance of hybrid stepper motors," IEEE Trans. Power Electron., vol. 32, no. 9, pp. 7244-7255, 2017.

[3] Y. Zhai, Y. Guo, L. Zhu, et al., "Simulation research on fuzzy PID closed-loop control system of stepping motor," Micromotors, vol. 38, no. 11, pp. 146-149, 2015.

[4] K. Ru, X. Guo, X. You, et al., "Open-loop high-speed control strategy of two-phase hybrid stepping motor," Power Electronics, vol. 51, no. 10, pp. 36-41, 2018.

[5] G. Cheng, Q. Ran and H. Ye, "Design of FPGA-based stepping motor subdivision control system," J. Wuhan Inst. Technol., vol. 40, no. 6, pp. 701, 2018.

[6] J. Shi, Stepping Motor Servo Control Technology. Beijing: Science Press, 2006.

[7] J. Liu, Advanced PID Control and MATLAB Simulation, 4th ed. Beijing: Publishing House of Electronics Industry, 2016.